Feedforward Control of Piezoactuators in Atomic Force Microscope Systems

KAM K. LEANG, QINGZE ZOU, and SANTOSH DEVASIA

INVERSION-BASED COMPENSATION FOR DYNAMICS AND HYSTERESIS

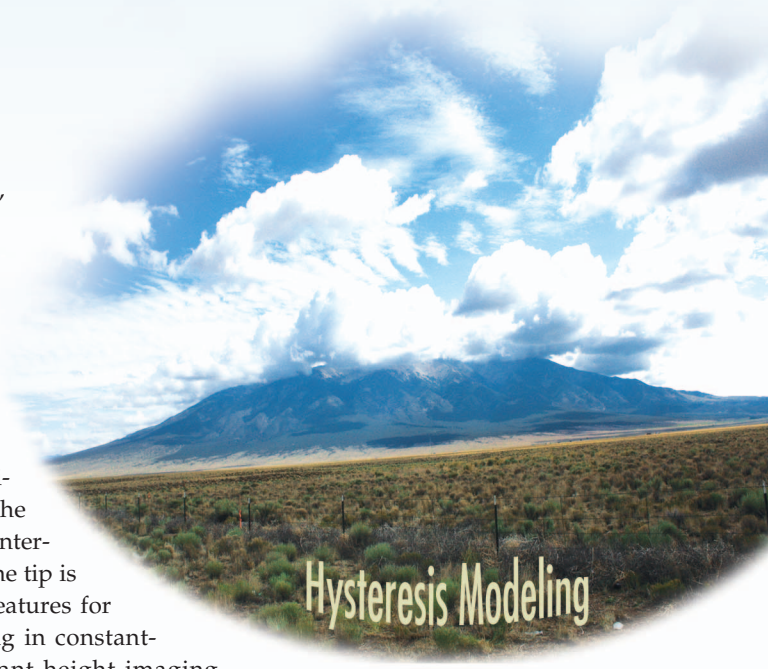

DENNIS S. BERNSTEIN

The atomic force microscope (AFM), a type of scanning probe microscope (SPM), is one of the foremost nanotechnology tools for interrogating, controlling, and manipulating matter at the nanoscale [1], [2]. The major components of the AFM are shown in Figure 1. At the heart of this instrument is a small microfabricated cantilever with a sharp tip (probe) located at its distal end. The cantilever, whose largest dimension is approximately several hundred micrometers, is barely visible to the naked eye. The AFM works by using the cantilever with a sharp tip as a force transducer to interact with matter at the nanoscale [3]. For instance, the tip is used as an indentation tool to create nanosized features for growing quantum dots [4] as well as for imaging in constant-height or constant-force mode [2]. In the constant-height imaging mode, the microcantilever and tip are rastered over a sample's surface at a constant height. Simultaneously, the vertical displacement of the cantilever, the movement of which is caused by tip-to-sample interaction, is measured and used to construct a three-dimensional image, with subnanometer resolution, of the surface topology. Therefore, the AFM is a unique tool for obtaining high-resolution topographical images, and it also has the ability to directly measure various properties of a specimen. For example, the structural and mechanical properties of biological specimens such as cells and DNA have been investigated by the AFM [5], [6], even in real time [7].

Most AFMs use piezoactuators, or piezopositioners, to move and position the cantilever probe relative to the sample surface in the lateral (x and y) and vertical (z) axes as shown in Figure 1 and Figure 2(a) and (b). The piezopositioner is made from piezoelectric material, a material that changes its dimensions when an electric field is applied to it. Compared to traditional actuators such as a dc motor, the piezoactuator is a solid-state device

Digital Object Identifier 10.1109/MCS.2008.930922

1066-033X/09/$25.00©2009IEEE

with a fast response, no moving parts, and no friction. The range of motion of a typical piezoactuator, for example, is in the lateral scanning direction in AFM, is approximately 100 μm, roughly the diameter of a human hair. Over this range the actuator can move with subnanometer resolution. But piezoactuators exhibit hysteresis and dynamic effects, the latter being creep and vibration, which make controlling their movements a challenge.

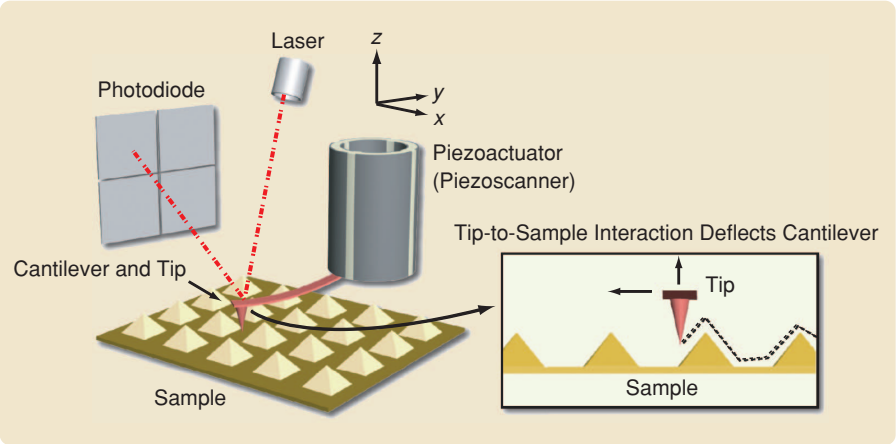

FIGURE 1 The key components of an atomic force microscope (AFM). The AFM operates by using a piezoactuator to scan a small microfabricated cantilever over the surface of a sample. The tip-to-sample interaction deflects the cantilever as it moves over the surface. The cantilever's deflection is measured by a laser and photodiode. The deflection can be used, for example, to create an image of the surface.

Precision positioning is needed in many AFM applications. In particular, precise position control in both the lateral and vertical directions is needed to hold the probe at a desired location or to track a desired motion trajectory. For instance, when the AFM is used to indent nanofeatures on a semiconductor surface to create quantum dots (2–80 nm in size), precise position control of the indenter tip is needed because the probe position error directly affects the size, spacing, and distribution of the nanofeatures. Even 2–4 nm variation in size and spacing of the nanofeatures can drastically alter their properties [8]. Moreover, high-speed control of the probe's movement is needed for high throughput fabrication, imaging, and metrology. Without precise motion control along a specific trajectory at high speed, oscillations can cause the tip to collide with nearby features, which leads to excessive tip-to-sample forces. The large forces can damage the probe or soft specimens such as live cells. Therefore, precise output tracking, or positioning, is critical in AFM. The objective of this article is to describe the method of inversion-based feedforward control for precise positioning of piezoactuators in AFMs. Specifically, the discussion addresses the issue of

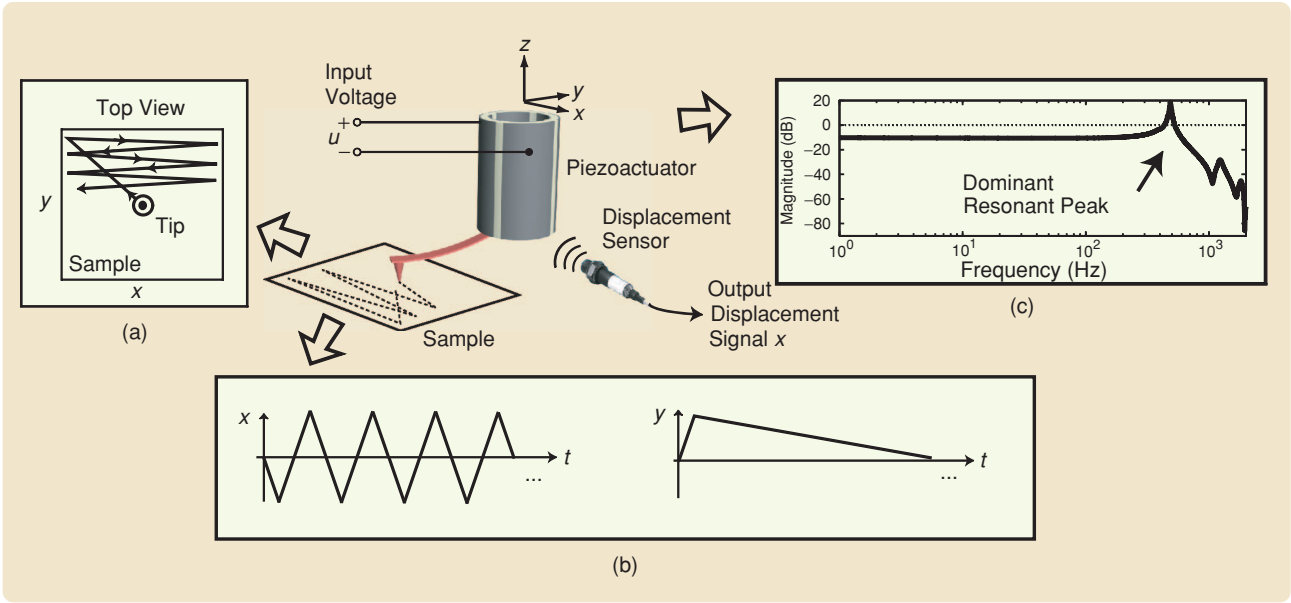

FIGURE 2 The movement of the piezoactuator and cantilever in atomic force microscope (AFM) imaging. (a) A top view of the AFM scan path that shows the tip's path during imaging. The tip starts at the center of the sample and then moves to the upper left-hand corner. From the corner, the tip rasters back and forth across the sample in the x direction. At the same time the tip moves slowly in the y direction during imaging. (b) The lateral x and y scan paths versus time. The movement of the piezoactuator in the x direction is significantly faster than the movement in the y direction. (c) The frequency response of the piezoactuator dynamics in the x direction, where the input is the applied voltage u and the output is the displacement signal x. The frequency response shows a sharp resonant peak. The sharp resonant peak limits the open-loop operation of the AFM to low frequencies.

inverting a dynamics model to account for vibration and creep and then inverting a hysteresis model to compensate for hysteresis in piezoactuators. Some attention is given to alternative methods for dealing with hysteresis, such as using high-gain feedback control and iterative control.

THE EFFECTS OF DYNAMICS AND HYSTERESIS ON AFM IMAGING

The precision and operating speed of AFMs are limited by essentially two major issues, dynamic and hysteresis effects of the piezoactuator. Other considerations, such as the cantilever dynamics and the dynamics of the mechanical fixtures that connect the cantilever to the piezoactuator, are also important. For example, in AFM imaging and force-curve measurements, the dynamics of the AFM between the piezoactuator voltage and the cantilever deflection along the z-axis include the dynamics of the piezoactuator, the AFM cantilever, and the mechanical fixtures.

The dynamic effects in piezoactuators include movement-induced oscillation, called vibration, and the creep effect. The amount by which the dynamics affect the output response of the piezoactuator depends on the input's frequency. When the input frequency is close to the resonance frequencies, vibration becomes noticeably large in the piezoactuator's output response. The large vibration is caused by exciting the resonant modes of the actuator [9]. Piezoactuators tend to be highly resonant structures due to their high stiffness and low structural damping. As a result, a sharp peak appears in the frequency response as illustrated in Figure 2(c). Therefore, input signals such as sawtooth signals can excite the piezoactuator's resonances, causing the output to oscillate or vibrate as shown in Figure 3(a).

Oscillations in the piezoactuator's lateral response can cause artifacts, such as ripples, which distort the resulting AFM images as depicted in Figure 3(b). To illustrate the source of these ripples, consider that the AFM cantilever and tip are rastered back and forth along the x-axis while simultaneously moving slowly from top-to-bottom along the y-axis [Figure 2(a) and (b)]. As the probe moves from left to right, the cantilever's vertical response is recorded at a constant sampling rate. Each value is associated with a desired probe position (x_d, y_d). The existence of lateral positioning error between the probe's desired and true position means that a cantilever's recorded vertical response does not agree with the expected lateral position. This discrepancy produces image distortion; in particular, the repeating vertically aligned corrugated appearance (ripples) in the image in Figure 3(b) is due to the repetitive nature of the lateral oscillations, from one scan line to the next. Also, such positioning errors can cause distortions in fabricated features when the AFM is used for nanofabrication.

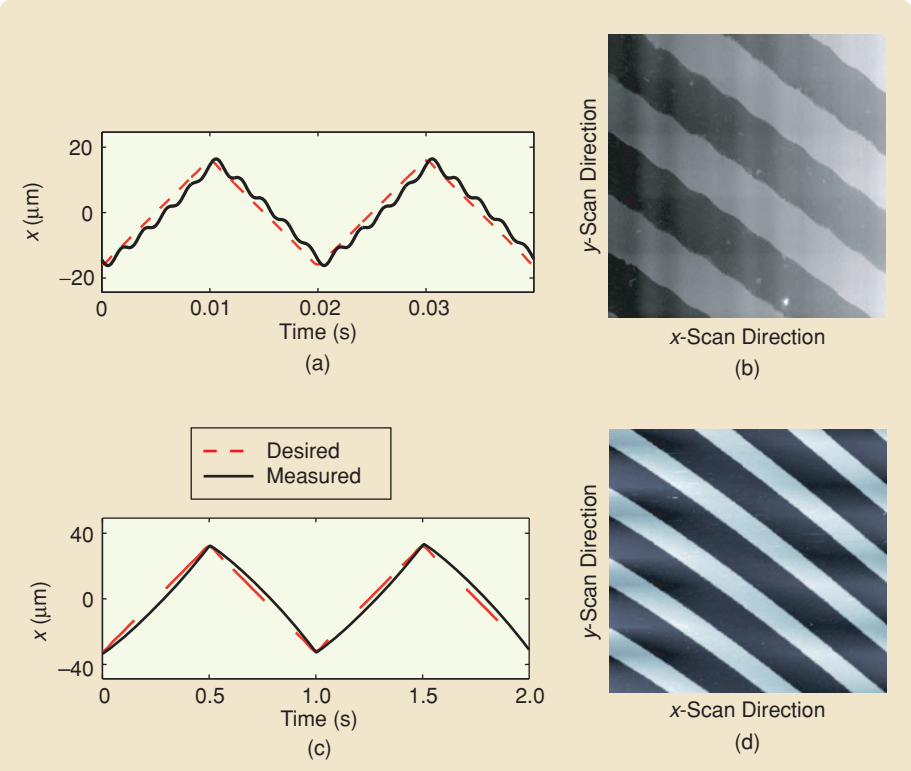

FIGURE 3 Distortion due to dynamic and hysteresis effects in atomic force microscope (AFM) imaging. (a) A plot of the measured displacement of the piezoscanner versus time at 50 Hz. The high-frequency scanning at 50 Hz excites the vibrational dynamics. The dynamics cause oscillations, which appear in the output displacement. (b) An AFM image taken at high frequency, which shows ripples caused by the vibrational dynamics. (c) A plot of the piezoscanner's measured displacement versus time for scanning at 1 Hz over a large range of ± 30 μm. The curved shape in the measured response is caused by hysteresis. (d) An AFM image taken at 1 Hz over a large range, which shows the distortion caused by hysteresis. The actual features are parallel.

One approach for avoiding vibration is to operate the piezoactuator at low speed. Scan speeds that are 20–100 times lower than the frequency of the dominant resonant peak are typically used [10]. This limitation, however, renders the AFM ineffective for high-speed applications. Another approach for improving the operating speed of the AFM is to use stiffer piezoactuators that have higher resonance frequencies [7], [11]. By shifting the resonance frequency to a higher value, the scan frequency at which vibration is significant becomes higher. The major

drawback, however, is that the range of motion of stiffer piezoactuators is reduced.

Feedback control can help reduce the vibration effect at high operating speeds [12]–[14]. Unfortunately, there are several challenges. First, piezoactuators have low structural damping, which results in low stability margins [15]. Second, feedback control is sensitive to sensor noise, which can limit the achievable precision.

At slow operating speeds, creep is a major source of positioning error. Creep in piezoactuators is a low-frequency behavior, where the output drifts, especially when the operation is offset from the center of the piezoactuator's positioning range. Without creep compensation, the AFM cannot be used for slow and static applications. For instance, creep makes it difficult to precisely fabricate nanofeatures using AFMs when the process time scale is on the order of minutes [16]. Creep in piezoactuators is analogous to creep in mechanics, where a constant load causes a material to slowly deform [17]. In the case of piezos, however, creep manifests itself as a remnant polarization that slowly increases after the onset of an electric field. Creep is negligible when the piezoactuator is operated at sufficiently high frequency [10].

Finally, hysteresis is significant over large-range displacements [12]. Hysteresis, which is a nonlinear behavior between the applied electric field and the mechanical displacement of the piezoactuator, is believed to be caused by irreversible losses that occur when similarly oriented electric dipoles interact upon application of an electric field [18]. An example of hysteresis is shown in Figure 3(c), where a 1-Hz triangular input signal is applied to the AFM piezoactuator and the measured output (± 30 μm) shows hysteresis-caused distortion. The distortion in the piezoactuator output then leads to distortion in an AFM image as shown in Figure 3(d). The actual features are parallel, but because of hysteresis they appear curved. Another aspect of hysteresis is that the output depends on the input history, known as the memory effect [19]. Therefore, between some initial and final time, two identical inputs can yield completely different output responses. This discrepancy occurs because of differences in the histories of the inputs prior to the initial time.

Operating piezoactuators in their linear range helps avoid hysteresis. In general, the linear range tends to be within 10% of the maximal range of motion. Charge control, as opposed to voltage control, of a piezoactuator is an alternative method for minimizing the hysteresis effect. This approach requires the design of a charge-feedback circuit [20]. Also, the Preisach approach is studied in [21]–[24] for hysteresis compensation.

The hysteresis and dynamic effects are coupled [10]. For instance, when the movement of the piezoactuator is large and slow, the piezoactuator exhibits hysteresis and creep effects. As the frequency of the input increases, the piezoactuator's output response shows the addition of the vibrational dynamics as large oscillations and ripples begin to appear. Therefore, the coupled behaviors make precise control of the AFM probe a daunting task. These coupled effects can be addressed with feedforward control based on a cascade model. Next, the cascade model is discussed, followed by describing an inversion-based feedforward method for dynamics and hysteresis compensation.

INVERSION-BASED FEEDFORWARD CONTROL OF DYNAMIC AND HYSTERESIS EFFECTS

Unlike feedback control, which reacts to the measured tracking error, feedforward control compensates or anticipates for deficit performance. A feedforward controller does this by exploiting a priori information about the system, and thus a well-designed feedforward controller requires sufficient knowledge of the plant dynamics and nonlinearities. In this case, the models are inverted to compensate for dynamic and hysteresis effects.

AFM applications can be divided into two categories, those that involve nonrepeating trajectories and those based on repeating motion. Applications with nonrepeating trajectories include nanofabrication and nanomanipulation, where the probe tip is required to track a user-defined trajectory once or a few times. Applications with repeating trajectories include imaging, where the piezoactuator is used to scan or raster a probe tip back and forth across a sample surface. The scanning motion in this case repeats from one cycle to the next. The main difference between the two categories is the ability to use iterative methods for the repeating motion case as outlined in Figure 4.

A Cascade Model for Feedforward Control

Inversion-based feedforward control exploits information about the system. Therefore, an input-output model for the piezoactuator is needed. The effects of vibrational dynamics, creep, and hysteresis on the output of a piezoactuator are intertwined. To model these behaviors, the cascade model depicted in Figure 5(a) and (b) is used. The range-dependent hysteresis effect is treated as a rate-independent, input nonlinearity represented by $\mathcal{H}$. The vibrational dynamics and creep effects are captured by the linear dynamics model $G(s)$. The cascade model structure is used extensively to model piezoactuators and similar systems [10], [25].

To find the feedforward input for precision output tracking, each submodel is inverted. More specifically, the feedforward control input u_{ff} is obtained by passing the desired output trajectory y_d through the inverse models of the dynamics and hysteresis in reverse order as illustrated in Figure 6.

An Inversion-Based Feedforward Approach for Dynamic Compensation

Described next is an inversion-based feedforward approach that compensates for the dynamic effects. Here,

the dynamics include vibration and the creep effect. The objective is to find a feedforward input $u_{ff}(t)$ by inverting the model $G(s)$ for precision tracking of the desired trajectory $y_d(t)$. One key feature of this feedforward approach is that it can be applied to nonminimum-phase systems [26]–[28]. Although the dynamic effects are specifically addressed in this section, the approach can be combined with alternative feedforward or feedback methods that compensate for hysteresis when the range of motion becomes large [15].

Let $G(s)$ represent the transfer function of the piezoactuator's dynamics, where the input is the applied voltage and the output is the displacement. Consider the minimal state-space realization of $G(s)$, given by

$$\dot{x}(t) = Ax(t) + Bu(t), \tag{1}$$

$$y(t) = Cx(t), \tag{2}$$

where $x(t)$ is the state vector, $u(t)$ is the input, and $y(t)$ is the output, for example, the displacement along one lateral (x or y) axis. To simplify the presentation, the piezoactuator system is assumed to be single-input, single-output (SISO). This approach is equally applicable to multi-input, multi-output (MIMO) systems. To find the feedforward input $u_{ff}(t)$ that exactly tracks the desired output $y_d(t)$ of the system (1), (2), the output equation (2) is differentiated until the input appears explicitly in the expression. Hence,

$$y^{(r)}(t) = CA^r x(t) + CA^{r-1}Bu(t), \tag{3}$$

where $CA^{r-1}B \neq 0$, r is the relative degree of the system (1), (2), and the superscript (r) denotes the rth time derivative. For a SISO system, the relative degree r is the difference between the number of poles and zeros of $G(s)$. Thus, the inverse feedforward input $u_{ff}(t)$ that tracks the desired trajectory $y_d(t)$ can be obtained directly from (3) by replacing $y(t)$ with the desired output $y_d(t)$, that is,

$$u_{ff}(t) = (CA^{r-1}B)^{-1}\left[y_d^{(r)}(t) - CA^r x_{\text{ref}}(t)\right]. \tag{4}$$

The inverse feedforward input (4) shows that finding the inverse input $u_{ff}(t)$ is equivalent to finding the reference states $x_{\text{ref}}(t)$. In other words, a bounded solution for $x_{\text{ref}}(t)$ is needed.

Under a state transformation, a portion $\xi_d(t)$ of the reference states $x_{\text{ref}}(t)$ is specified by the desired output and its derivatives, up to $r-1$ derivatives. Thus, for a given desired trajectory, $\xi_d(t)$ is known. Then it remains to find the unknown reference states $\eta(t)$ to determine the feedforward input (4).

The unknown reference states $\eta(t)$ are found by solving the associated dynamics for a given desired output trajectory $y_d(t)$. The inverse input (4) is substituted back into (1), (2) and then rewritten in the transformed coordinate $[\xi_d,\ \eta]^T$. The unknown reference state equation becomes [28]

$$\dot{\eta}(t) = \hat{A}_\eta \eta(t) + \hat{B}_\eta \mathbf{Y}_d(t), \tag{5}$$

where $\mathbf{Y}_d(t)$ is the vector consisting of the desired output $y_d(t)$ and its derivatives up to the rth order. The details

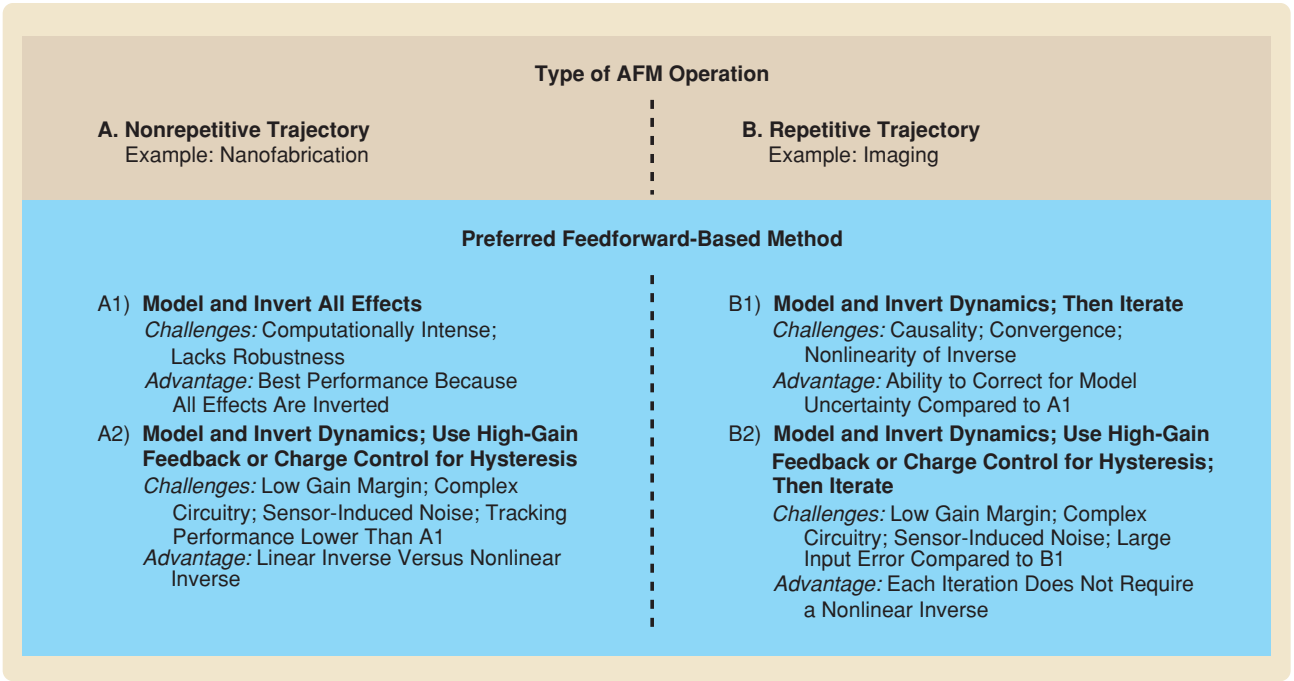

FIGURE 4 An overview of inversion-based feedforward. The left column describes the preferred feedforward method for AFM applications that involve nonrepetitive trajectories. The right column deals with applications that involve repetitive trajectories and in which control based on iteration is allowed.

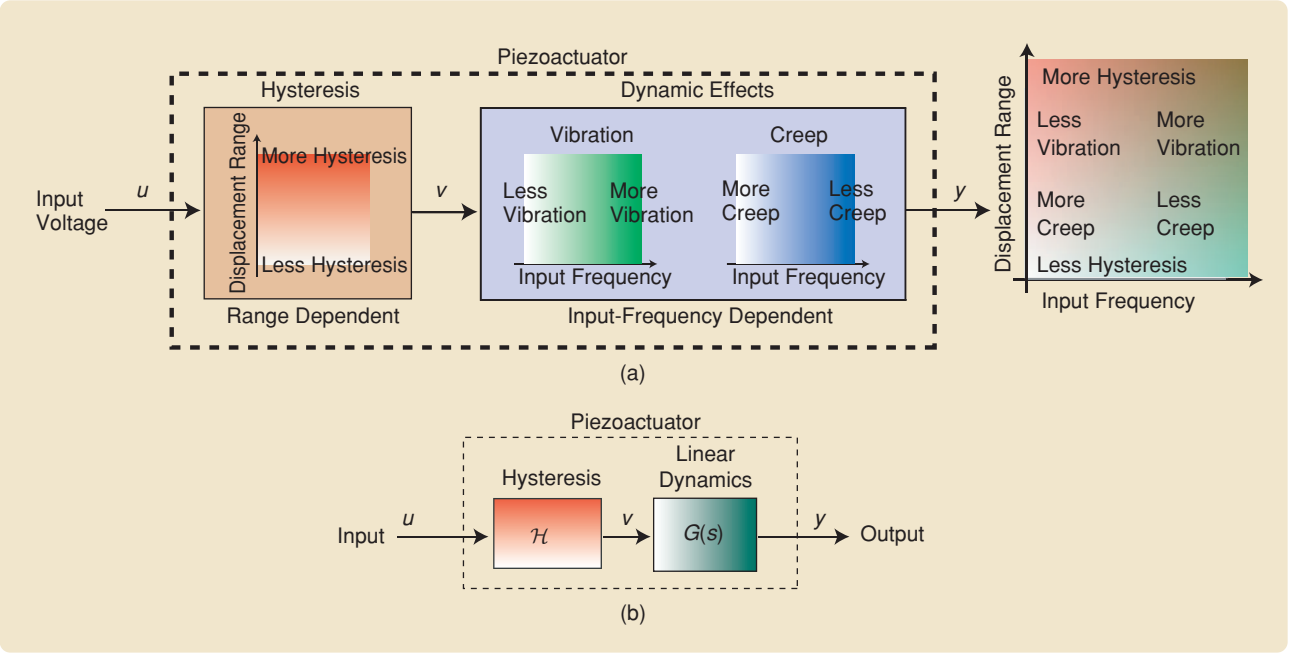

FIGURE 5 A cascade model structure for hysteresis, vibrational dynamics, and creep effects in piezoactuators. (a) This model shows the three effects as separate blocks. Hysteresis is modeled as an input nonlinearity that is output-range dependent. The input-frequency-dependent vibrational dynamics and creep effects follow the hysteresis block. (b) The block diagram of the cascade model. The hysteresis is denoted by $\mathcal{H}$, while the linear dynamics model $G(s)$ captures the vibrational dynamics and creep effect.

about $\hat{A}_\eta$ and $\hat{B}_\eta$ can be found in [28]. Equation (5) constitutes the *internal dynamics* of system (1), (2).

It can be shown, for example in [29], that the poles of the internal dynamics (5) are exactly the zeros of (1). Therefore, if the system is nonminimum phase, the internal dynamics (5) are unstable, and the goal is to find a bounded solution to the internal dynamics $\eta(t)$. This objective is addressed by the stable inversion theory [27], [28].

Stable inversion of unstable internal dynamics is based on the concept of noncausality. The internal dynamics (5) of a system without any zeros on the imaginary axis can be decoupled into the stable σ_s and unstable σ_u dynamics through a state transformation, that is,

$$\dot{\sigma}_s = A_s\sigma_s(t) + B_s\mathbf{Y}_d(t), \tag{6}$$

$$\dot{\sigma}_u = A_u\sigma_u(t) + B_u\mathbf{Y}_d(t). \tag{7}$$

See [30] for the case of systems that have pure imaginary zeros.

The stable internal dynamics (6) are associated with the minimum-phase zeros, that is, the eigenvalues of A_s in (6) lie in the open left-half complex plane. Likewise, the unstable internal dynamics (7) are associated with the nonminimum-phase zeros, that is, the eigenvalues of A_u in (7) are in the open right-half complex plane. Then the bounded solution to the unstable part of the internal dynamics can be solved by flowing the dynamics backwards in time,

$$\sigma_u(t) = -\int_t^\infty e^{\bar{A}_u(t-\tau)}\hat{B}_u\mathbf{Y}_d(\tau)d\tau. \tag{8}$$

Therefore, (8) implies that to obtain the current value of the internal dynamics as well as the current value of the inverse input (4), the desired output trajectory must be specified in advance; thus, the stable inversion is noncausal. In many applications, such as the lateral scanning trajectory for AFM imaging, the desired trajectory is known a priori. For applications in which the desired trajectory is not completely known in advance, a preview-based stable inversion approach can be used [28], [31]. Basically, the preview-based approach computes the inverse input using the desired trajectory within a finite time window. Finite preview of the desired trajectory is feasible in many applications. For example, in AFM-based nanomanipulation and

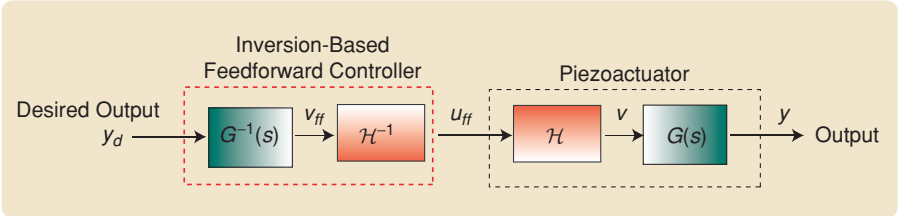

FIGURE 6 An inversion-based feedforward approach to compensate for dynamic and hysteresis effects. The feedforward control input u_{ff} is obtained by passing the desired output trajectory y_d through the inverse models of the hysteresis and dynamics in reverse order.

nanofabrication, it may be required to drive the AFM-probe to follow a real-time, user-specified trajectory. Therefore, finite preview of the future desired trajectory is available, and the preview-based inversion technique is applicable. In short, this technique tracks the user's motion with a delay time that equals the preview time. This delay is usually acceptable in nanomanipulation applications.

The Optimal Inverse Approach

The inversion-based method presented above may yield excessively large inputs when the system has lightly damped system zeros. These large inputs can saturate the voltage amplifiers that drive the piezoactuator, or, even worse, depole the piezoactuator. Additionally, large model uncertainties around the resonant peaks or lightly damped zeros can cause significant error in computing the feedforward input. These model uncertainties thus lead to a lack of robustness when the inversion-based feedforward method is used. The following optimal inversion approach is used to account for these issues. Specifically, an optimal feedforward input is obtained by minimizing the quadratic cost function [32]

$$J(u) = \int_{-\infty}^{\infty} \{u^*(j\omega)R(j\omega)u(j\omega) + [x(j\omega) - x_d(j\omega)]^* Q(j\omega)[x(j\omega) - x_d(j\omega)]\} d\omega, \quad (9)$$

where * denotes conjugate transpose and $R(j\omega)$ and $Q(j\omega)$ are nonnegative, frequency-dependent real-valued weights on the input energy and the tracking error, respectively. The optimal feedforward input $u_{ff,\mathrm{opt}}$ that minimizes (9) is

$$u_{ff,\mathrm{opt}}(j\omega) = \left[\frac{G^*(j\omega)Q(j\omega)}{R(j\omega) + G^*(j\omega)Q(j\omega)G(j\omega)}\right] y_d(j\omega). \quad (10)$$

By choosing the frequency-dependent weights $R(j\omega)$ and $Q(j\omega)$, it is possible to systematically consider the effects of the input magnitude and the model uncertainties. For instance, the input energy weight $R(j\omega)$ can be chosen to be much larger than the tracking error weight $Q(j\omega)$ at frequencies where large model uncertainties exist or around lightly damped zeros. For details and implementation issues, see [33] and [34].

Inversion-Based Feedforward Hysteresis Compensation

The Preisach hysteresis model [19] has been studied extensively to characterize rate-independent hysteresis in piezoelectric materials [24] as well as many hysteretic systems, including shape memory alloy devices [35]. This model assumes that the output $v(t)$ of a hysteretic system is the sum of weighted elementary relays $\mathcal{R}$ as given by

$$v(t) = \mathcal{H}[u](t) \triangleq \iint_{\alpha \geq \beta} \mu(\alpha, \beta)\mathcal{R}_{\alpha,\beta}[u](t)\, d\alpha\, d\beta, \quad (11)$$

where $\mu(\alpha, \beta)$ is the weighting value associated with the elementary relay $\mathcal{R}_{\alpha,\beta}$. Each relay can switch between two states, specifically, $+1$ and -1, depending on the value of the input u. The switching between the states $+1$ and -1 occurs when the input exceeds a relay's lower or upper switching threshold, β and α, respectively, where it is assumed that $\alpha \geq \beta$. The relays represent, for example, the switching behavior of individual electric dipoles within the piezoelectric material [36]. See [19] for a detailed discussion of the Preisach model and its properties.

The Preisach hysteresis model can be obtained experimentally from measured output data, for instance, by applying an appropriate input voltage and measuring the piezoactuator's displacement. Several approaches are available for estimating the Preisach weighting surface $\mu(\cdot, \cdot)$ from the data [35], [37]. One approach is to generate a collection of first-order descending (FOD) curves, compile the curves into a FOD surface, and then differentiate the FOD surface to find an estimate of the Preisach weighting surface $\mu(\cdot, \cdot)$ [19]. Although the method is straightforward, the differentiation process can amplify noise in the measured data, thus creating significant error. An alternative, and more favorable approach, is to find $\mu(\cdot, \cdot)$ by discretizing the Preisach plane and using a least squares technique to determine the values of μ at a finite number of locations in the Preisach plane $\mathbf{P} \triangleq \{(\alpha, \beta) | \alpha \geq \beta; \underline{u} \leq \alpha; \beta \leq \bar{u}\}$, where $\underline{u}$ and $\bar{u}$ are the minimal and maximal input values, respectively [37], [38].

Rather than invert the Preisach model for feedforward compensation of hysteresis, an inverse-Preisach model can be found directly from the measured input and output data. The inverse model is found using the same method to find the traditional Preisach model; however, the roles of the input and output are reversed. It is shown in [10] that when the input $u(t)$ is considered as the output and the output $v(t)$ is considered as the input, the inverse Preisach model takes the form

$$u(t) = \mathcal{H}^{-1}[v](t) \triangleq \iint_{\hat{\alpha} \geq \hat{\beta}} \gamma(\hat{\alpha}, \hat{\beta})\mathcal{R}_{\hat{\alpha},\hat{\beta}}[v](t)\, d\hat{\alpha}\, d\hat{\beta}, \quad (12)$$

where the parameters $\hat{\alpha}$, $\hat{\beta}$, $\gamma(\hat{\alpha}, \hat{\beta})$, and the elementary relay $\mathcal{R}_{\hat{\alpha},\hat{\beta}}$ are associated with the inverse-Preisach model. Like the traditional Preisach model, it is assumed that the nonlinearity operates within closed major loops; therefore, the weighting function $\gamma(\hat{\alpha}, \hat{\beta})$ is zero outside of the upper triangle defined by the boundaries $\hat{\alpha} = \hat{\beta}$, $\hat{\alpha} = \bar{v}$, and $\hat{\beta} = \underline{v}$, where $\bar{v}$ and $\underline{v}$ are the upper and lower bounds on the output, respectively.

With the inverse model in hand, a desired output trajectory is passed through the inverse model to generate an input that compensates for hysteresis effect. The results of this technique for AFM are presented below.

Inversion-Based Feedforward Hysteresis and Dynamics Compensation

When an AFM application calls for large-range and high-speed motion, both hysteresis and dynamics compensation are required for precision output tracking. In this case, the feedforward control input $u_{ff}(t)$, which accounts for both the dynamic and hysteresis effects, is obtained by passing the desired output trajectory $y_d(t)$ through the inverse models in reverse order as depicted in Figure 6. This process is performed offline, followed by applying the feedforward input to the piezoactuator. First, the dynamic inverse produces an output $v_{ff}(t)$. The output from this first stage then becomes the input to the inverse-Preisach model, which produces the final feedforward input $u_{ff}(t)$ to compensate for both hysteresis and dynamics.

AFM IMAGING APPLICATION

Modeling the Dynamic Effects

The transfer function models for the vibrational dynamics and creep effects are obtained by curve fitting the measured frequency and time responses of the piezoactuator over appropriate frequency ranges.

The experimental results described herein come from a piezoactuator (piezoscanner) in a Burleigh AFM. Lateral positioning is achieved using a tube-shaped piezoactuator with quarter-sectored electrodes, which enable control of the positioning in the x and y axes (see Figure 7). The positioning of the AFM probe in the vertical z-axis is controlled by a separate piezoactuator. The vertical motion control is not considered here, but rather the focus is on controlling the lateral motion of the piezoactuator for AFM imaging. The piezoactuator's lateral movements are measured with optical displacement sensors with submicron resolution.

To find the vibrational dynamics model, which relates the input u to the displacement x or y, the first step is to measure the frequency response using a dynamic signal analyzer. The response is measured over a displacement range of less than 10% of the maximal range to avoid the hysteresis effect. To avoid creep, the response is measured over a wide frequency range, in this case, 1 Hz to 2 kHz. The solid line in Figure 8 shows the measured frequency response curve for the piezoactuator in the x axis.

Using a system identification algorithm, such as the function "invfreqs" in Matlab, a transfer function model is fitted to the measured response. The dash line shown in Figure 8 is the model given by (13), as shown at the bottom of the page.

At very low speed, the creep effect is significant. This effect can be described by the Kelvin-Voigt model, which consists of spring (k_i) and damper (c_i) elements [39]. The lumped-parameter model shown in Figure 9 is linear, and its transfer function is

$$G_c(s) = \frac{x(s)}{u(s)} = \frac{1}{k_0} + \sum_{i=1}^{n} \frac{1}{sc_i + k_i}, \tag{14}$$

where $x(s)$ is the displacement of the piezoactuator and $u(s)$ is the applied input voltage. In (14), k_0 models the elastic behavior at dc, and the creep behavior is captured by selecting an appropriate model order corresponding to the number of spring-damper elements n. The parameters k_0, k_i, and c_i of (14) are determined by curve fitting the step response of the piezoactuator over, for example, a three-minute period as shown in Figure 9. The second-order model ($n = 2$) in Figure 9 is

$$G_c(s) = \frac{0.4s^2 + 9.9s + 7.5}{s^2 + 20.9s + 14.7}. \tag{15}$$

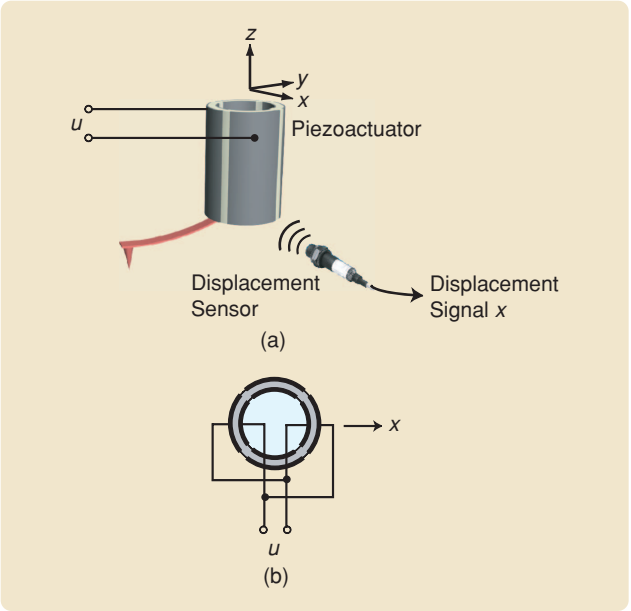

FIGURE 7 An electrode configuration for a tube-shaped piezoactuator in an atomic force microscope. (a) The input voltage u drives the piezoactuator in the x direction. The x-direction displacement is measured by an optical or inductive sensor. (b) The wiring diagram shows how the electrodes are connected to the piezoactuator.

Vibrational Dynamics Compensation

To illustrate the application of the inversion-based approach for dynamics, the vibrational dynamics model $G_v(s)$ is inverted to find a feedforward input $u_{ff}(t)$ that tracks a given desired trajectory $x_d(t)$, that is, the desired trajectory along the fast-scanning x-axis. In the experiments the range of motion is less than 10% of the maximal range. Over this range, the hysteresis effect is negligible. The desired scan frequency is chosen greater than 1 Hz to reduce the creep effect.

$$G_v(s) = \frac{7.2 \cdot 10^{13}s^2 + 2.3 \cdot 10^{16}s + 3.2 \cdot 10^{21}}{s^6 + 1.1 \cdot 10^4 s^5 + 9.5 \cdot 10^7 s^4 + 7.0 \cdot 10^{11}s^3 + 2.0 \cdot 10^{15}s^2 + 5.6 \cdot 10^{18}s + 1.0 \cdot 10^{22}}. \tag{13}$$

The fast scanning axis in the x direction tends to be 100 times faster than the motion in the y axis during AFM imaging. For instance, a 100×100 pixel image implies that the probe rasters back and forth across the sample 100 times per image acquired (see Figure 2 for the scan pattern). Therefore, the fast scanning motion in the x direction excites the mechanical resonances of the piezoactuator, causing the output to oscillate. The oscillations subsequently cause unwanted ripple-like distortion to appear in the AFM image as described above.

To compensate for the dynamic effects, the inversion-based approach is used to determine a feedforward input to be applied to the piezoactuator. Figure 10 shows the feedforward control scheme, along with the AFM imaging results over the small range for (b) without feedforward compensation and (c) with feedforward compensation. The inversion process for a prespecified desired trajectory is directly implemented in frequency domain using the fast Fourier transform (FFT) algorithm in Matlab. In the experiment, the range of motion is approximately 10 μm to minimize the hysteresis effect. Figure 10(a) shows ripples caused by the vibrational dynamics for a 30-Hz scan. Lightly colored vertical bands are evident of the vibration effects. When the

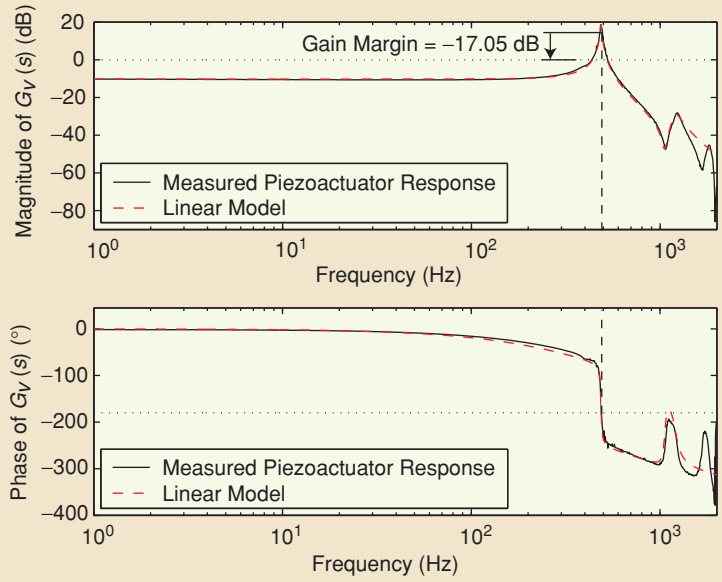

FIGURE 8 The frequency response of a piezoactuator for modeling the vibrational dynamics. These plots show the measured frequency response (solid line), the magnitude and phase versus frequency of the piezoactuator over ± 2-μm displacement range. The dash line is the linear vibrational dynamics model.

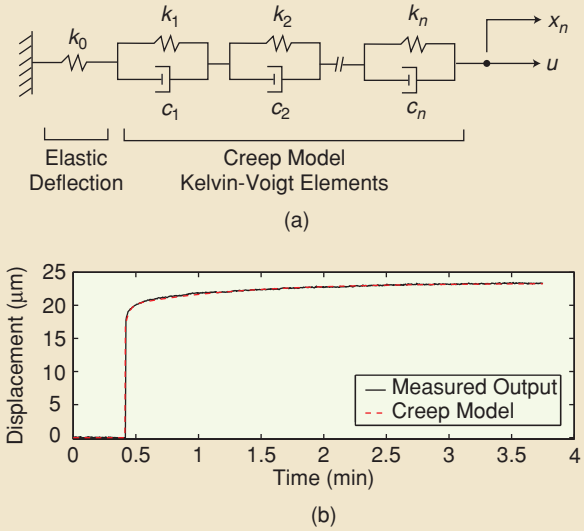

FIGURE 9 Modeling the creep effect in a piezoactuator. (a) The spring-damper model is used to model the creep effect. The parameters of the model are found by curve fitting the measured step response of the piezoactuator. (b) The time response shows the measured step response (solid line) and the linear creep model (dashed line).

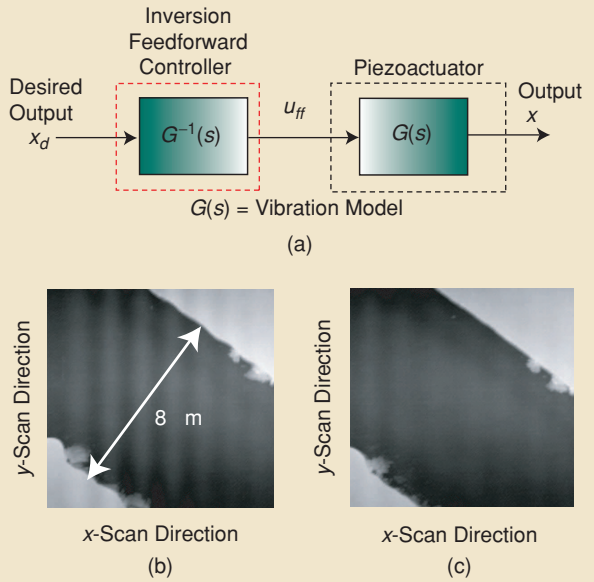

FIGURE 10 Feedforward control of the linear vibrational dynamics to achieve high-speed positioning over small range. The (a) block diagram shows the feedforward control scheme, where the linear vibrational dynamics model $G(s)$ is inverted to compensate for vibration effects. The atomic force microscope images are acquired (b) without feedforward compensation and (c) with feedforward compensation. The feedforward input reduces the ripples caused by vibration.

feedforward input is applied, the image shows significantly fewer ripples. In particular, the edges that separate the light and dark regions in the image show less oscillations in their appearance. Artifacts caused by minute particles on the sample's surface along the black/white edges and in the lower left-hand corner can be seen in both images.

Feedforward Dynamics and Hysteresis Compensation

The vibrational dynamics, creep, and hysteresis effects are accounted for using the inversion-based approach as presented in the control scheme shown in Figure 11. Both the dynamic and hysteresis effects are inverted for precision positioning. In particular, the optimal inverse is used to compute the feedforward input for a given desired output trajectory $x_d(t)$. Then, the computed input is passed through the inverse-Preisach model to generate the feedforward input $u_{ff}(t)$. The resulting input compensates for dynamic and hysteresis effects. The image in Figure 11(b) is acquired without feedforward compensation. The features appear slightly curved because of hysteresis and the ripples show the effect of the dynamics. These distortions are compensated for by applying the feedforward input $u_{ff}(t)$ to the piezoactuator as shown by Figure 11(c).

Feedforward and High-Gain Feedback Control

Modeling and inverting the dynamic and hysteresis effects are effective methods for precision positioning in AFM [10], [33]. However, because the approach exploits knowledge of the piezoactuator behavior, the modeling process can be time consuming, particularly when both the inverse dynamics and inverse hysteresis are used. If a simpler method to account for hysteresis is preferred over the control performance, then high-gain feedback can be used to linearize the nonlinear behavior of the piezoactuator. The vibrational dynamics are modeled, inverted, and combined with the feedback controller as shown in Figure 12. However, when feedback is used, piezoactuators often exhibit low gain margin and can cause instability. For example, the frequency response of the piezoactuator depicted in Figure 8 shows a −17.05-dB gain margin. This low gain margin is attributed to the low structural damping and higher order dynamics (poles) that combine to pull the system's phase response below the −180° mark. Therefore, the feedback gain is severely limited, and a high-gain closed-loop system can potentially become unstable.

Gain margin can be improved by cascading the piezoactuator with a notch filter $D(s)$, which cancels the effect of the sharp resonant peak [15]. In Figure 12, the notch filter raises the gain margin, for example from −17.05 to 30.86 dB, enabling the use of high gain feedback to minimize the hysteresis behavior.

With the improved gain margin, a proportional-derivative (PD) feedback controller is combined with the feedforward controller for AFM imaging. Proportional-integral-derivative

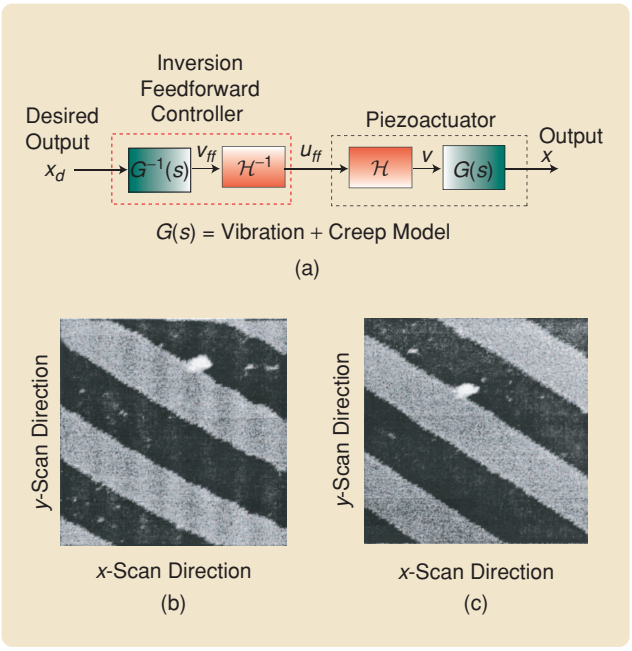

FIGURE 11 Feedforward control of dynamics $G(s)$ and hysteresis $\mathcal{H}$ for large-range, low- and high-speed positioning. The (a) feedforward control input $u_{ff}(t)$ is obtained by passing the desired output trajectory $x_d(t)$ through the inverse models of hysteresis and dynamics in reverse order. The atomic force microscope images are acquired (b) without feedforward compensation and (c) with feedforward compensation. The feedforward input minimizes hysteresis, vibration, and creep. (These images from [10] are presented with permission from ASME.)

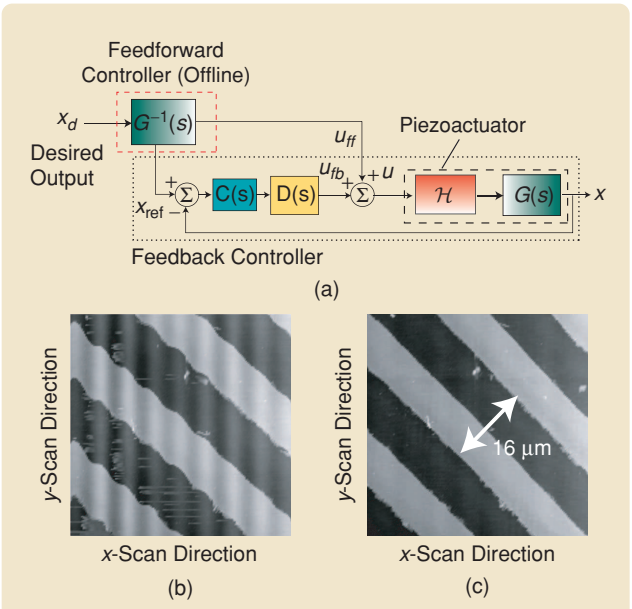

FIGURE 12 Integrated feedforward and feedback controller for dynamics $G(s)$ and hysteresis $\mathcal{H}$. The integrated controller achieves high-speed positioning over a large range. The (a) block diagram shows a feedback controller for minimizing hysteresis and a feedforward controller for compensating for the vibrational dynamics. The atomic force microscope images are acquired (b) without feedforward compensation and (c) with feedforward compensation. The integrated controller accounts for distortions due to both hysteresis and vibration.

feedback controllers can also be used [12], [14]. The results of the feedback and feedforward controller are shown in Figure 12. A scan of a calibration sample over a large range with only PD feedback control is shown in Figure 12(b). Although hysteresis is not noticeable in the image, the effect of vibration is significant at a scan rate of 30 Hz. But when the feedforward input is added to the feedback-controlled system, the ripples are greatly reduced as shown in Figure 12(c). Therefore, the use of feedback with a feedforward input computed from the linear dynamics model avoids the need to model and invert the hysteresis behavior. The addition of feedback also improves the robustness to adverse effects including system dynamics variations and disturbances.

Validating the Cascade Model for Piezoactuators

The inversion-based feedforward approach can also be applied to validate the cascade model for modeling the dynamics and hysteresis in piezoactuators. First, when the displacement range of the piezoactuator is within the linear range, hysteresis is negligible, and the output exhibits only linear dynamics [10]. But when the piezoactuator is operated outside of its linear range, the inversion-based approach is applied to compensate for the hysteresis effect. In the end, the large- and small-range outputs are measured and compared to see whether the cascade model is acceptable.

The block diagram in Figure 13(a) outlines an experiment where hysteresis is compensated for by using an iteration-based method. The details of this method are described in [40]. First, a 100-Hz triangle input is applied to the piezoactuator, causing it to move over a small range of ± 1 μm. In this case, the output response shows oscillations caused by the vibrational dynamics because hysteresis is negligible over the small range [see Figure 13(b)]. Next, the feedforward input from the iteration-based approach that accounts for hysteresis is applied to track a 100-Hz triangle trajectory over a larger range of ± 25 μm. The output in this case is measured and denoted by v_1. Then the output v_1 is compared to the ± 1-μm-range output scaled by 25, denoted by $25v_2$, as shown in Figure 13(b). The maximum and root-mean-square of the difference $v_1 - 25v_2$ are 6.09 and 1.63% of the full ± 25-μm range, respectively. The small error values suggest that the cascade model is acceptable for modeling piezoactuators over the specific frequency range.

An additional experiment is performed to check whether the hysteresis is rate independent. The idea is to compensate for the dynamic effects at various frequencies and then compare the results. The experiment is described by the block diagram in Figure 14(a), where the output of the piezoactuator is passed through the inverse of the dynamics. The experimental details are covered in [40]. The results shown in Figure 14(b) compare the response

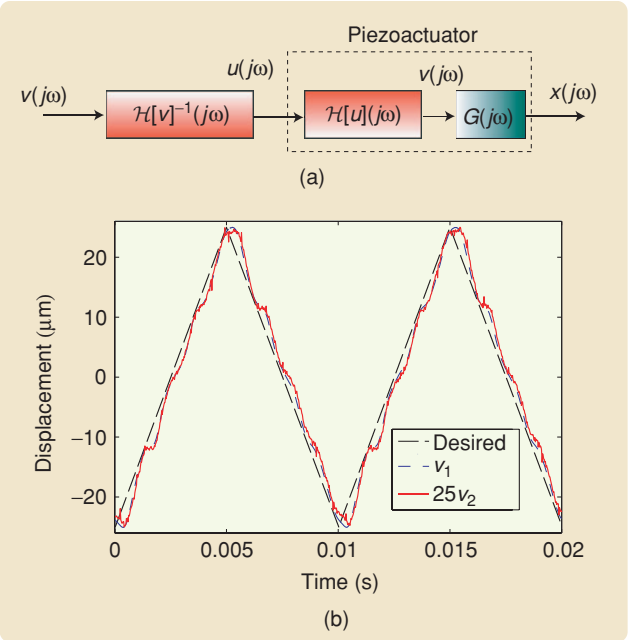

FIGURE 13 Experimental results for checking whether hysteresis is input-range dependent using the inversion-based approach. The (a) block diagram shows the control scheme used to compensate for hysteresis such that dynamic effects remain in the output. The (b) tracking response is measured over a large range (± 25 μm) at 100 Hz after the hysteresis is accounted for. Also shown is the small-range (± 1 μm) response scaled by 25 ($25v_2$) for comparison. The maximum and root-mean-square of the difference $v_1 - 25v_2$ are 6.09% and 1.63% of the full ± 25 μm range, respectively.

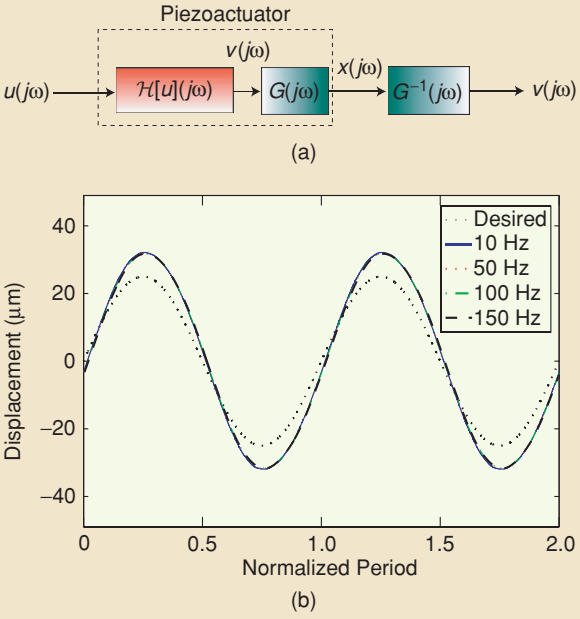

FIGURE 14 Experimental results for checking whether hysteresis is rate independent using the inversion-based approach. The (a) block diagram shows the control scheme used to compensate for the vibrational dynamics. The (b) time response shows the tracking performance for several frequencies (10, 50, 100, and 150 Hz), where the units of the horizontal axis are normalized periods of the output signal. At each frequency, the measured responses are within 2% of each other.

for tracking a sinusoidal signal $x_d(t) = A\sin(2\pi f t)$ with $A = 30$ μm and $f = 10, 50, 100, 150$ Hz. Because the dynamics are compensated for by using the inversion approach, the remaining distortions are caused by hysteresis. The maximum difference between the output for the four cases is less than 2% of the ± 30-μm range. The small error between the four frequencies suggests that the hysteresis effect is rate independent within the frequency range studied in the experiment.

Current Efforts in Inversion-Based Iterative Feedforward Control

One of the main challenges in implementing inversion-based feedforward control is the fact that a reasonably accurate system model is needed, or, alternatively, the model uncertainties and variations must be small. These issues can be addressed by two approaches. When the desired trajectory is known beforehand, one approach is to use inversion-based iterative control (IIC) [40]–[42]. An alternative approach is to use the robust inversion feedforward control method for tracking the desired trajectories online with finite preview [43], [44].

IIC introduces an iteration mechanism to find the feedforward input. The basic idea is to minimize the adverse effect of modeling errors or dynamics uncertainties by iteratively correcting the input from one trial to the next. Unlike conventional iterative learning control [45], IIC explicitly exploits the inverse model of the system dynamics. This approach is demonstrated in [40] and [46] for scanning and force-curve measurement in AFM applications. Also, the method can be used to deal with cross-coupling effects such as when the input in the x-axis excites the vertical motion of the piezoactuator in the z-direction at high frequency [41].

Finally, recent advances in iteration-based feedforward control for SPM include sensorless implementation [47] and iteration for hysteresis compensation [22]. For example, in nanoresolution SPM imaging using a scanning tunneling microscope, where a sensor for measuring the movement of the piezoactuator is not available, an image-based iterative control method is developed to account for dynamic effects [47]. The acquired images are used to extract the tracking error, and the estimated error is subsequently used to iteratively determine the inverse input. Also, an iteration method is developed to account for the hysteresis effect in [22] and for both hysteresis and dynamic effects in [40]. One of the main challenges with iterative methods for hysteresis compensation is showing convergence. The difficulty arises because of the multivalued nature of hysteresis, where multiple outputs exist for a given input value and vice versa. Therefore, the direction in which the input needs to be changed to reduce the output error cannot be uniquely determined. However, a method is discussed in [22] for convergence with guaranteed convergence rates.

CONCLUSIONS

This article describes an inversion-based feedforward approach to compensate for dynamic and hysteresis effects in piezoactuators with application to AFM technology. To handle the coupled behavior of dynamics and hysteresis, a cascade model is presented to enable the application of inversion-based feedforward control. The dynamics, which include vibration and creep, are modeled using linear transfer functions. A frequency-based method is used to invert the linear model to find an input that compensates for vibration and creep. The inverse is noncausal for nonminimum-phase systems. Similarly, the hysteresis is handled by an inverse-Preisach model. To avoid the complexity of finding the inverse-Preisach model, high-gain feedback control can be used to linearize the system's behavior. A feedforward input is then combined with the feedback system to compensate for the linear dynamics to achieve high-speed AFM imaging. Finally, recent efforts in feedforward control for an SPM application including the use of iteration to handle hysteresis as well as uncertainties and variations in the system model is discussed.

ACKNOWLEDGMENT

This research was funded through National Science Foundation grants DUE 0633098 and 0632908 and CMS 0196214 and 0336221.

REFERENCES

[1] R. Wiesendanger, *Scanning Probe Microscopy and Spectroscopy*. Cambridge, U.K.: Cambridge Univ. Press, 1994.
[2] S.M. Salapaka and M.V. Salapaka, "Scanning probe microscopy," *IEEE Control Syst. Mag.*, vol. 28, no. 2, pp. 65–83, 2008.
[3] I.W. Rangelow, "Scanning proximity probes for nanoscience and nanofabrication," *Microelectron. Eng.*, vol. 83, pp. 1449–1455, 2006.
[4] C. Taylor, E. Stach, A. Malshe, and G. Salamo, "Nanoscale dislocation patterning by ultralow load indentation," *Appl. Phys. Lett.*, vol. 87, pp. 73–108, 2005.
[5] M. Radmacher, "Measuring the elastic properties of biological samples with the AFM," *IEEE Eng. Medicine and Biol.*, vol. 16, pp. 47–57, 1997.
[6] S. Kasas, N.H. Thomson, B.L. Smith, P.K. Hansma, J. Miklossy, and H.G. Hansma, "Biological applications of the AFM: From single molecules to organs," *Int. J. Imaging Syst. and Technol*, vol. 8, no. 2, pp. 151–161, 1997.
[7] T. Ando, N. Kodera, D. Maruyama, E. Takai, K. Saito, and A. Toda, "A high-speed atomic force microscope for studying biological macromolecules in action," *Jpn. J. Appl. Phys. Part 1*, vol. 41, no. 7B, pp. 4851–4856, 2002.
[8] D. Leonard, M. Krishnamurthy, C.M. Reaves, S.P. Denbaars, and P.M. Petroff, "Direct formation of quantum-sized dots from uniform coherent islands of InGaAs on GaAs surfaces," *Appl. Phys. Lett.*, vol. 63, no. 23, pp. 3203–3205, 1993.
[9] D. Croft and S. Devasia, "Vibration compensation for high speed scanning tunneling microscopy," *Rev. Sci. Instr.*, vol. 70, no. 12, pp. 4600–4605, 1999.
[10] D. Croft, G. Shed, and S. Devasia, "Creep, hysteresis, and vibration compensation for piezoactuators: Atomic force microscopy application," *ASME J. Dyn. Syst., Meas., and Contr.*, vol. 123, pp. 35–43, 2001.
[11] G. Schitter, K.J. Astrom, B.E. DeMartini, P.J. Thurner, K.L. Turner, and P.K. Hansma, "Design and modeling of a high-speed AFM-scanner," *IEEE Trans. Contr. Syst. Technol.*, vol. 15, no. 5, pp. 906–915, 2007.
[12] R.C. Barrett and C.F. Quate, "Optical scan-correction system applied to atomic force microscopy," *Rev. Sci. Instr.*, vol. 62, no. 5, pp. 1393–1399, 1991.
[13] S. Salapaka, A. Sebastin, J.P. Cleveland, and M.V. Salapaka, "High bandwidth nano-positioner: A robust control approach," *Rev. Sci. Instr.*, vol. 73, no. 9, pp. 3232–3241, 2002.
[14] D.Y. Abramovitch, S.B. Anderson, L.Y. Pao, and G. Schitter, "A tutorial on the mechanisms, dynamics, and control of atomic force microscopes," in *Proc. American Control Conf.*, New York, 2007, pp. 3488–3502.
[15] K.K. Leang and S. Devasia. "Feedback-linearized inverse feedforward

for creep, hysteresis, and vibration compensation in AFM piezoactuators," *IEEE Trans. Contr. Syst. Technol.*, vol. 15, no. 5, pp. 927–935, 2007.
[16] S.M. Hues, C.F. Draper, K.P. Lee, and R.J. Colton, "Effect of PZT and PMN actuator hysteresis and creep on nanoindentation measurements using force microscopy," *Rev. Sci. Instr.*, vol. 65, no. 5, pp. 1561–1565, 1994.
[17] W.D. Callister, *Materials Science and Engineering: An Introduction.* New York: Wiley, 1994.
[18] D.C. Jiles and D.L. Atherton, "Theory of ferromagnetic hysteresis," *J. Magn. and Magn. Mater.*, vol. 61, pp. 48–60, 1986.
[19] I.D. Mayergoyz, *Mathematical Models of Hysteresis*. New York: Springer-Verlag, 1991.
[20] A.J. Fleming and K.K. Leang, "Charge drives for scanning probe microscope positioning stages," *Ultramicroscopy*, vol. 108, pp. 1551–1557, 2008.
[21] H. Janocha and K. Kuhnen, "Real-time compensation of hysteresis and creep in piezoelectric actuators," *Sensors and Actuators A*, vol. 79, pp. 83–89, 2000.
[22] K.K. Leang and S. Devasia, "Design of hysteresis-compensating iterative learning control for piezo positioners: Application to atomic force microscopes," *Mechatronics*, vol. 16, pp. 141–158, 2006.
[23] R.V. Iyer, X. Tan, and P.S. Krishnaprasad, "Approximate inversion of the Preisach hysteresis operator with application to control of smart actuators," *IEEE Trans. Automat. Contr.*, vol. 50, no. 6, pp. 798–810, 2005.
[24] P. Ge and M. Jouaneh, "Modeling hysteresis in piezoceramic actuators," *Precision Eng.*, vol. 17, no. 3, pp. 211–221, 1995.
[25] X. Tan and J.S. Baras, "Adaptive identification and control of hysteresis in smart materials," *IEEE Trans. Automat. Contr.*, vol. 50, no. 6, pp. 827–839, 2005.
[26] E. Bayo, "A finite-element approach to control the end-point motion of a single-link flexible robot," *J. Robotic Syst.*, vol. 4, pp. 63–75, 1987.
[27] S. Devasia, D. Chen, and B. Paden, "Nonlinear inversion-based output tracking," *IEEE Trans. Automat. Contr.*, vol. 41, no. 7, pp. 930–942, 1996.
[28] Q. Zou and S. Devasia, "Preview-based stable-inversion for output tracking," *ASME J. Dyn. Syst. Meas. Contr.*, vol. 121, no. 4, pp. 625–630, 1999.
[29] A. Isidori, *Nonlinear Control Systems*, 3rd ed. New York: Springer-Verlag, 1995.
[30] S. Devasia, "Output tracking with nonhyperbolic and near nonhyperbolic internal dynamics: Helicopter hover control," *AIAA J. Guid., Contr., and Dyn.*, vol. 20, no. 3, pp. 573–580, 1997.
[31] Q. Zou and S. Devasia, "Preview-based stable-inversion for output tracking of nonlinear nonminimum-phase systems: The VTOL example," *Automatica.*, vol. 41, no. 1, pp. 117–127, 2007.
[32] J.S. Dewey, K.K. Leang, and S. Devasia, "Experimental and theoretical results in output-trajectory redesign for flexible structures," *ASME J. Dyn. Syst., Meas., and Contr.*, vol. 120, pp. 456–461, 1998.
[33] S. Tien, Q. Zou, and S. Devasia, "Preview-based optimal inversion for output tracking: Application to scanning tunneling microscopy," *IEEE Trans. Contr. Syst. Technol.*, vol. 12, no. 3, pp. 375–386, 2004.
[34] Q. Zou, "Optimal preview-based stable-inversion for output tracking of nonminimum-phase linear systems," in *Proc. IEEE Conf. Decision and Control,* New Orleans, LA, Dec. 2007, pp. 5258–5263.
[35] S. Majima, K. Kodama, and T. Hasegawa, "Modeling of shape memory alloy actuator and tracking control system with the model," *IEEE Trans. Contr. Syst. Technol.*, vol. 9, no. 1, pp. 54–59, 2001.
[36] P. Ge and M. Jouaneh, "Tracking control of a piezoceramic actuator," *IEEE Trans. Contr. Syst. Technol.*, vol. 4, no. 3, pp. 209–216, 1996.
[37] X. Tan, R. Venkataraman, and P.S. Krishnaprasad, "Control of hysteresis: Theory and experimental results," *SPIE Modeling, Signal Processing and Contr. Smart Structures*, vol. 4326, 2001, pp. 101–112.
[38] W.S. Galinaitis and R.C. Rogers, "Control of a hysteretic actuator using inverse hysteresis compensation," in *SPIE Conf. on Mathematics and Control in Smart Structures*, vol. 3323, 1998, pp. 267–277.
[39] L.E. Malvern, *Introduction to the Mechanics of a Continuous Medium.* Englewood Cliffs, NJ: Prentice-Hall, 1969.
[40] Y. Wu and Q. Zou, "Iterative control approach to compensate for both the hysteresis and the dynamics effects of piezo actuators," *IEEE Trans. Contr. Syst. Technol.*, vol. 15, pp. 936–944, 2007.
[41] S. Tien, Q. Zou, and S. Devasia, "Control of dynamics-coupling effects in piezo-actuator for high-speed AFM operation," *IEEE Trans. Contr. Syst. Technol.*, vol. 3, no. 6, pp. 921–931, 2005.
[42] Q. Zou, C. Vander Giessen, J. Garbini, and S. Devasia, "Precision tracking of driving waveforms for inertial reaction devices," *Rev. Sci. Instr.*, vol. 76, no. 1, pp. 23701–23709, 2005.
[43] S. Devasia, "Should model-based inverse input be used as feedforward under plant uncertainty?," *IEEE Trans. Automat. Contr.*, vol. 47, no. 11, pp. 1865–1871, 2002.
[44] Y. Wu and Q. Zou, "Robust-inversion-based 2DOF-control design for output tracking: Piezoelectric actuator example," in *Proc. IEEE Conf. Decision and Control,* New Orleans, LA, Dec. 2007, pp. 2451–2457.
[45] K.L. Moore, M. Dahleh, and S.P. Bhattacharyya, "Iterative learning control: A survey and new results," *J. Robotic Syst.*, vol. 9, no. 5, pp. 563–594, 1992.
[46] K.-S. Kim, Q. Zou, and C. Su, "A new approach to scan-trajectory design and tracking: AFM force measurement example," *ASME J. Dyn. Syst., Meas., and Contr.*, vol. 130, pp. 051005-1–051005-10, 2008.
[47] G.M. Clayton and S. Devasia, "Image-based compensation of dynamic effects in scanning tunneling microscopes," *Nanotechnol.*, vol. 16, pp. 809–818, 2005.

AUTHOR INFORMATION

Kam K. Leang (kam@unr.edu) received the B.S. and M.S. degrees in mechanical engineering from the University of Utah, Salt Lake City, Utah, in 1997 and 1999, respectively, and the Ph.D. degree from the University of Washington, Seattle, Washington, in 2004. He joined the Department of Mechanical Engineering at the University of Nevada-Reno in 2008. From 2005 to 2008, he taught in the Mechanical Engineering Department at Virginia Commonwealth University, Richmond. His research interests include modeling and control of piezoactuators for scanning probe microscopy applications, fabrication and control of electroactive polymers, mechatronics, and design of microelectromechanical systems for nanotechnology. He is a member of ASME, IEEE, and SPIE. He can be contacted at the Department of Mechanical Engineering, University of Nevada-Reno, Mail stop 312, Reno, NV 89557-0312 USA.

Qingze Zou received the B.S. degree in automatic control from the University of Electronic Science and Technology of China (UESTC), Chengdu, in 1994, the M.S. degree in mechanical engineering from Tsinghua University, Beijing, in 1997, and the Ph.D. degree in mechanical engineering from the University of Washington, Seattle, in 2003. He was a research associate in the Department of Mechanical Engineering, University of Washington, from 2003 to 2004. Since 2004, he has been an assistant professor at the Department of Mechanical Engineering, Iowa State University at Ames. His research interests are in inversion-based output tracking theory, high-speed imaging of soft materials and characterization and modeling of rate-dependent material properties using scanning probe microscope, and high-throughput nanomanufacturing. He is a member of ASME and IEEE.

Santosh Devasia received the B.Tech. (Hons) from the Indian Institute of Technology, Kharagpur, in 1988 and the M.S. and Ph.D. degrees in mechanical engineering from the University of California at Santa Barbara in 1990 and 1993, respectively. He is a professor in the Mechanical Engineering Department at the University of Washington, Seattle, which he joined in 2000. From 1994 to 2000, he taught in the Mechanical Engineering Department at the University of Utah, Salt Lake City. He is an associate editor for the *ASME Journal of Dynamic Systems, Measurement and Control* and *IEEE Transactions on Control Systems Technology*. His research interests include inversion-based control theory for nanotechnology and biomedical applications, such as the imaging of human cells to investigate cell locomotion, and the control of distributed systems such as air traffic management.